Electronic Supplementary Material (ESI) for Physical Chemistry Chemical Physics.

SUPPORTING INFORMATION

Pt nanocluster size effects in the hydrogen evolution reaction: Approaching the theoretical maximum activity

Jens Klein[1], Albert K. Engstfeld[1,+], Sylvain Brimaud[2,*], R. Jürgen Behm[*,1]

[1]Institute of Surface Chemistry and Catalysis, Ulm University,

Albert-Einstein-Allee 47, D-89081 Ulm, Germany

[2]Zentrum für Sonnenenergie- und Wasserstoff-Forschung Baden-Württemberg (ZSW),

Helmholtzstrasse 8, D-89081 Ulm, Germany

* authors to whom correspondence should be addressed: juergen.behm@uni-ulm.de, sylvain.brimaud@zsw-bw.de

\+ pres. address: Institute of Electrochemistry, Ulm University, Albert-Einstein-Allee 47, D-89081 Ulm, Germany

1 Overview on previous experimental HER studies on Pt nanoclusters

Table S1: Summary of the results of previous experimental HER studies on Pt NCs, with focus on NC sizes ranging from single atom catalysts (SACs) to 2 nm. SAC studies are only listed when included in the NC study.

Particle size effect							
Particle size	**Most active**	**Support**	**Mass activity**	**j_o**	**Theory**	**Stability**	**Ref**
0.23 nm - 10.12 nm	N/A (0.46 nm - 3.04 nm)	Bi, Pb	N/A	N/A	N/A	Deactivation after first HER cycle	1
Pt_1, Pt_{10}, Pt_{13}, 230 nm	Pt_{13} atoms	TiO_2/Ti	229 A mg_{Pt}^{-1} @ -0.60 V	N/A	N/A	SA: Agglomeration NCs: Dissolution	2
Pt_3, Pt_{15}, Pt_{30}, Pt_{45},	Pt_{30} / Pt_{45}	$SrTIO_3$(100)	N/A	N/A	N/A	Agglomeration	3
3.8 nm, 4.7 nm, 5.3 nm	3.8 nm	Glassy carbon	N/A	0.9 mA cm^{-2}	N/A	N/A	4
2.1 nm, 3.3 nm, 4.4 nm, 8.7 nm	2.1 nm		100 A mg_{Pt}^{-1} (exchange current)	135 mA cm^{-2}	N/A	N/A	5
Pt_{25}, Pt_{33}, Pt_{38}, Pt_{49}, Pt_{99}, Pt_{110}	Pt_{38}	gr/Ru(0001)	5.27 A mg_{Pt}^{-1} @ 0.01 V	10.1 mA cm^{-2}	N/A	Slight deactivation after 3 cycles	Own work
Pt-mass-specific Activity							
Catalyst	**Support**	**Mass-specific activity**	**j_o**	**Theory**	**Stability**	**Ref**	
Pt NP	Vulcan XC-72	0.27 A mg_{Pt}^{-1} @ -0.05 V	N/A	Yes	Deactivation @ 0.04 V	6	
Pt NP (20 wt%)	Vulcan XC-72R E-Tek	0.03 A mg_{Pt}^{-1} @ -0.10 V	1.5 mA cm^{-2}	N/A	N/A	7	
Pt NP (7.5 wt%)	W_2C	0.07 A mg_{Pt}^{-1} @ -0.10 V	2.1 mA cm^{-2}	N/A	N/A	7	
ALD-50-Pt	N-doped graphene nanosheets	10.1 A mg_{Pt}^{-1} @ -0.05 V	N/A	Yes	Stable @ 0.04 V	6	
SAC	Single walled CNT	N/A	1.94 mA cm^{-2}	Yes	Stable after 5000 cycles	8	
SAC	CoP-Nanotubes on Ni foam	70 A g_{Pt}^{-1} @ -0.05 V	N/A	N/A	Stable after 5000 cycles	9	
SAC	Aniline-stacked graphene	22.4 A mg_{Pt}^{-1} @ -0.05 V	4.56 mA cm^{-2}	Yes	Stable after 2000 cycles	10	
3.5 nm	DNA	1.33 A mg_{Pt}^{-1} @ -0.045 V	N/A	N/A	1000 min @ -0.035 V	11	
SAC	PyPOP@G	0.37 A mg_{Pt}^{-1} @ -0.05 V	N/A	N/A	Stable after 1250 cycles	12	
Pt_3Ni_2 nanowires-S	Carbon	3.25 A mg_{Pt}^{-1} @ -0.07 V	N/A	Yes	N/A	13	

2 Experimental set-up

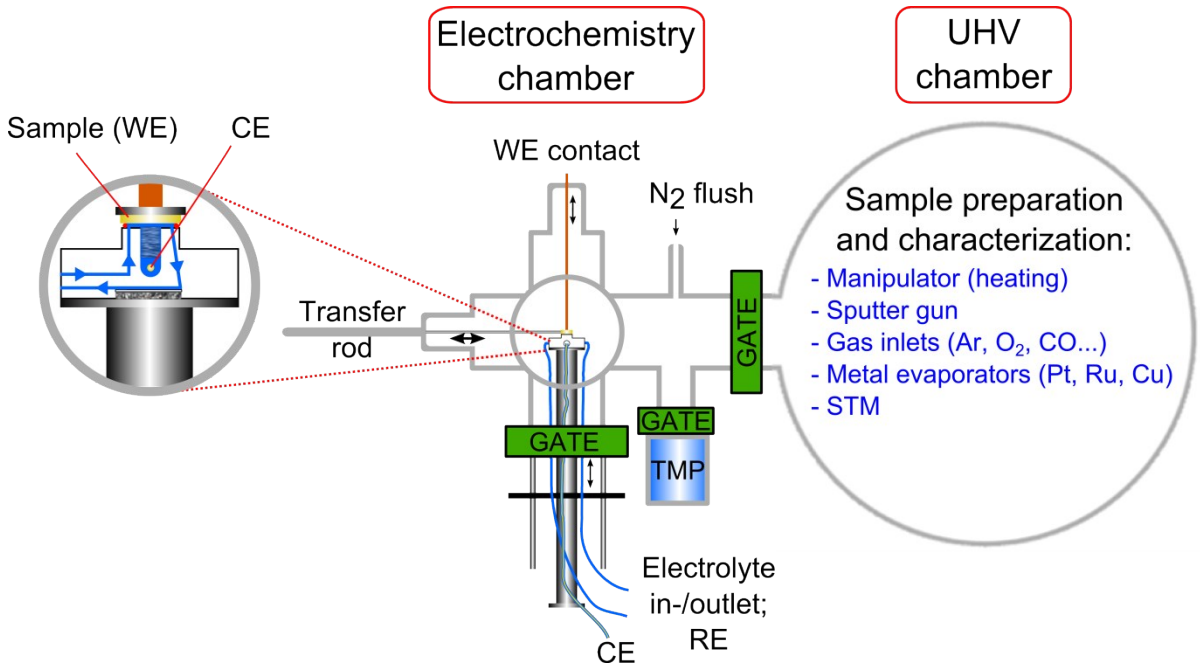

Figure S1: Schematic illustration of the combined UHV-STM-EC flow cell set-up. For more details see Ref. [14].

3 Electrochemical properties and stability of gr/Ru(0001)

The cyclic voltammograms (CV) for bare Ru(0001) and gr/Ru(0001) electrodes in supporting electrolyte are compared in Fig. S2. The CV of Ru(0001) exhibits characteristic current features for surface oxidation and reduction processes which were already described in detail in Ref. [15]. This contains a broad oxidation peak in the positive-going scan initiated at 0.45 V and two reduction peaks centered at 0.52 V and 0.32 V. The CV of the gr/Ru(0001) electrode shows an almost complete suppression of these potential-induced surface oxidation/reduction current features, indicating a successful coverage of the Ru(0001) by the graphene layer. Nonetheless, we note a tiny reduction peak at 0.32 V, which might be attributed to the reduction of surface Ru oxide of non-covered Ru(0001). The coulometric charge under this peak equals 2 μC cm^{-2} whereas the charge of the peak at 0.32 V on the bare Ru(0001) electrode is 131 μC cm^{-2}. This indicates that ca. 98.5% of the Ru(0001) single crystal is covered by the graphene layer, which can be rated as defect free.

On both Ru(0001) and gr/Ru(0001), the hydrogen evolution reaction is initiated at ca. 0.10 V. At -0.02 V, the current density for the HER is about 10 μA cm^{-2} for both electrodes, which is far below the current densities measured for the Pt-gr/Ru(0001) electrodes being in the mA cm^{-2} range. Thus, the contribution from the gr/Ru(0001) substrate is considered as negligible. Fig. S2b shows an STM image recorded after electrochemical measurements. The periodic buckling of the Moiré is still clearly visible and no defects were observed in the grapheme layer. Therefore, there is no restructuring of graphene in the potential range where the HER is performed on the Pt-gr/Ru(0001) electrodes.

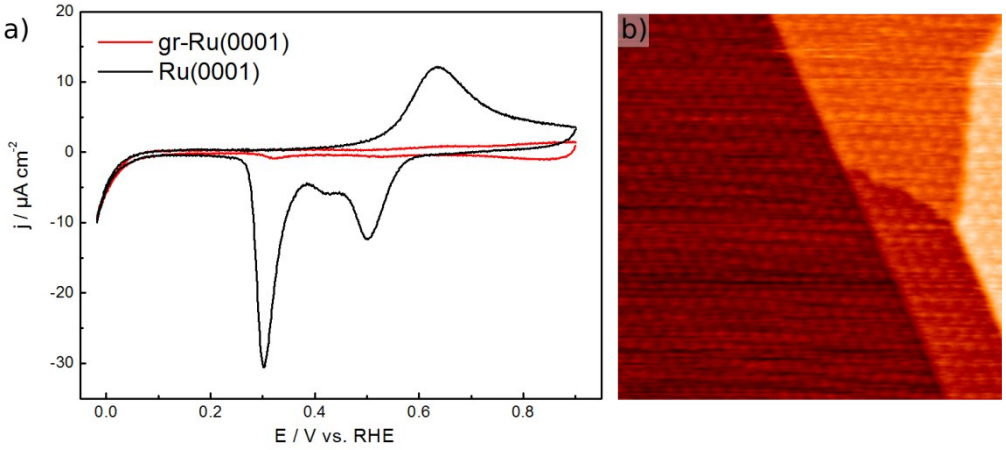

Figure S2: (a) Cyclic voltammograms of Ru(0001) (black) and gr/Ru(0001) (red) in 0.5 M H_2SO_4 (10 mV s^{-1}). (b) Representative STM image of gr/Ru(0001) recorded after electrochemical measurements (70 nm x 70 nm).

4 Size control of Pt NCs on gr/Ru(0001)

The nucleation and growth behavior of Pt NCs on gr/Ru(0001) was already studied extensively in previous studies.[16-19] Based on these studies we tuned the size of the Pt NCs as described in the following. For NCs with sizes below 1 nm we deposited Pt on gr/Ru(0001) with a constant evaporation rate (0.03 ML min^{-1}) at room temperature. The size of the Pt NCs was increased by increasing the Pt coverage (θ_{Pt}), i.e., by increasing the evaporation duration. Accordingly, the Pt coverage was varied from θ_{Pt} = 0.02 ML to θ_{Pt} = 0.12 ML for electrode **1** to **3** (see Fig. 1b in the main text and Table S2). For even larger Pt NCs we first deposited Pt with a coverage of θ_{Pt} = 0.12 ML on gr/Ru(0001) at room temperature. Subsequently, the samples were annealed to a specific temperature (T_{sint}), which led to ripening of the Pt NCs.[20] Accordingly, we annealed the electrodes **4** to **6** to temperatures between T_{sint} = 473 K to T_{sint} = 873 K subsequent to the Pt deposition at room temperature (see Fig. 1b in the main text and Table S2).

As depicted in Fig. S3, which presents representative STM images and corresponding NC height distributions of the different electrodes, we obtained by the above described preparation procedure, six electrodes with increasing Pt NC size from electrode **1** to **6**. For the electrodes **1** to **5** the NC height distributions are very narrow compared to commercial Pt/C catalyst materials thanks to the gr/Ru(0001) template (The broader height distribution of electrode **6** is discussed below). The most abundant Pt NC height h_{max} for electrode **1** is h_{max} = 1-2 ML_{Pt} while it is h_{max} = 3 ML_{Pt} for electrode **3** (see also Table S2). Post-annealing of the electrodes **4-6** led to a continuous increase of h_{max}.

The so-called filling factor FF, which is defined as the ratio of the number of Pt NCs to the overall amount of existing fcc-Moiré adsorption sites,[17,20] was determined by statistical

analysis of the Pt NCs in a total area containing 1350 to 2240 fcc-Moiré sites and the resulting values are given in Table S2. Since the distance between two adsorption sites for the Pt NCs on the gr/Ru(0001) substrate is 3 nm, there are one hundred adsorption site within a 30 nm x 30 nm unit cell. Thus, the NC density can be calculated by dividing the FF value by the respective area in this unit cell (779.4 nm²). The values of the respective NC densities are given in Table S2. Increasing the Pt coverage from θ_{Pt} = 0.02 ML to θ_{Pt} = 0.12 ML led to an increase of the FF / NC density for the electrodes **1-3**. As expected, the FF / NC density then decreased for the electrodes **4** to **6** with increasing annealing temperature due a ripening process.

Table S2: Structural characteristics and electrocatalytic properties of the Pt-gr/Ru(0001) electrodes.

Electrode	θ_{Pt} [ML]	$T_{sint.}$ [K]	FF [%]	$\rho_{Cluster}$ [$\cdot 10^{12}$ cm^{-2}]	h_{max} [ML_{Pt}]	S_{av} [atoms]
1	0.02	298	14.4	1.85	1-2	25
2	0.06	298	27.0	3.47	2-3	33
3	0.12	298	37.2	4.77	3	38
4	0.12	473	32.1	4.12	4	49
5	0.11	673	12.7	1.63	4-5	99
6	0.12	873	3.19	0.41	2-12	110

Pt coverage (θ_{Pt}), annealing temperature ($T_{sint.}$), filling factor (FF) cluster density ($\rho_{Cluster}$), most abundant cluster height (h_{max}), and average number of Pt atoms per cluster (S_{av}) for each electrode.

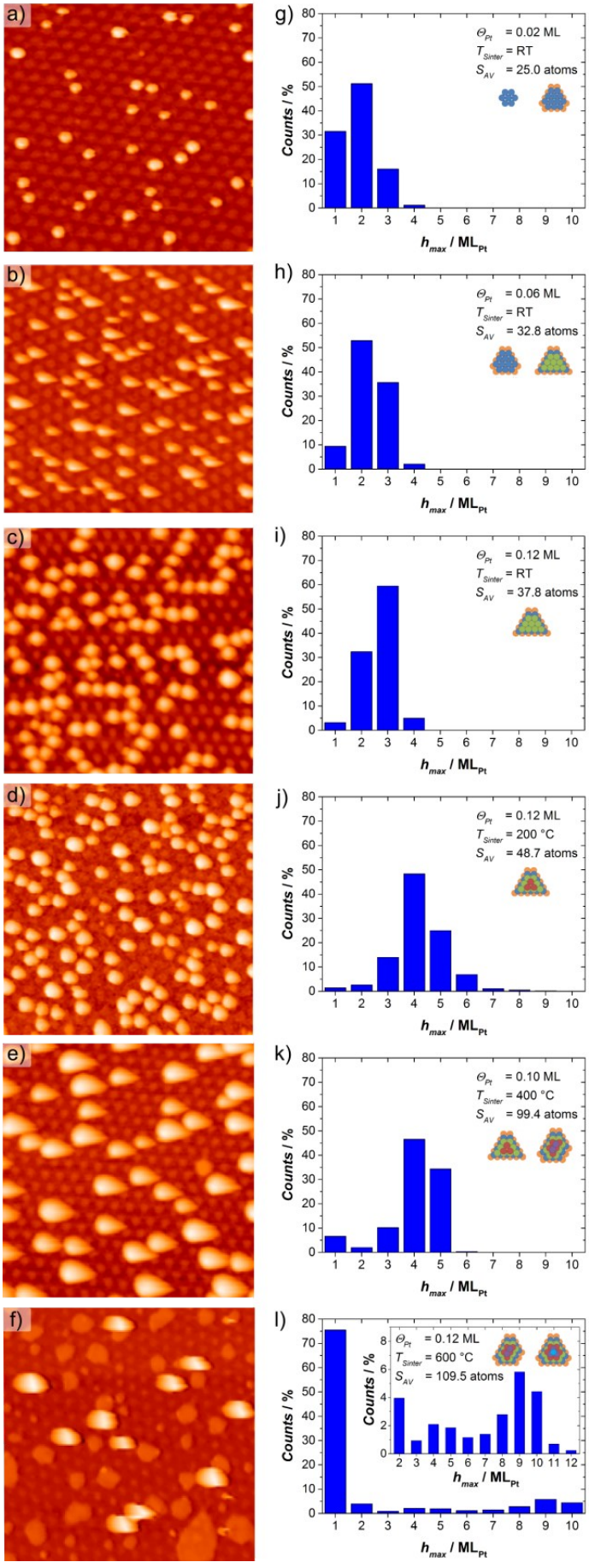
a)
b)
c)
d)
e)
f)
g)
h)
i)
j)
k)
l)
Θ_{Pt} = 0.02 ML
T_{Sinter} = RT
S_{AV} = 25.0 atoms
Θ_{Pt} = 0.06 ML
T_{Sinter} = RT
S_{AV} = 32.8 atoms
Θ_{Pt} = 0.12 ML
T_{Sinter} = RT
S_{AV} = 37.8 atoms
Θ_{Pt} = 0.12 ML
T_{Sinter} = 200 °C
S_{AV} = 48.7 atoms
Θ_{Pt} = 0.10 ML
T_{Sinter} = 400 °C
S_{AV} = 99.4 atoms
Θ_{Pt} = 0.12 ML
T_{Sinter} = 600 °C
S_{AV} = 109.5 atoms
Counts / %
h_{max} / ML_{Pt}

Figure S3: (a) - (f): STM images (50 nm x 50 nm) of the six different Pt-gr/Ru(0001) with a coverage of (a) θ_{Pt} = 0.02 ML (I_T = 0.089 nA, U_T = 1.75 V), (b) θ_{Pt} = 0.06 ML (I_T = 0.013 nA, U_T = 2.3 V) and (c) θ_{Pt} = 0.12 ML (I_T = 0.013 nA, U_T = -1.3 V) and subsequent annealing to (d) T_{Sint} = 473 K (θ_{Pt} = 0.12 ML) (I_T = 0.028 nA , U_T = 0.7 V), (e) T_{Sint} = 673 K (θ_{Pt} = 0.10 ML) (I_T = 0.013 nA , U_T = 2.3 V) and T_{Sint} = 873 K (θ_{Pt} = 0.12 ML) (I_T = 0.631 nA, U_T = 1.5 V). (g) - (l): Respective height distributions. The heights are given in multiples of one monolayer height of Pt (ML_{Pt}). In each height profile the respective θ_{Pt}, the annealing temperature T_{Sint}, the average number of atoms per Pt NC (S_{AV}) and cluster models of the most abundant Pt NCs are shown. (l): The inset shows the same height distribution without h_{max} = 1 ML_{Pt}.

A closer inspection of the STM image of electrode **6** in Fig. S3 reveals two different kinds of nanostructures on the surface: bright NCs with heights in the range of 2-12 ML_{Pt} and monolayer high Pt islands (less bright) exceeding the size of a single Moiré adsorption site. For a better characterization of these islands a zoom in of such an island is depicted in Fig. S4a. In this image the corrugation of the graphene sheet as well as two bright spots on top of the 1 ML high Pt-island are observed where the latter exhibit the same distance as two γ-regions of the corrugated graphene sheet. A height profile along the blue line in Fig. S4a is depicted in Fig. S4b. The island width along the blue line is around d = 6 nm and the height from the lowest part of the island (at d = 8.9 nm) to the lowest point of the graphene corrugation was determined to be h = 2.26 Å which is equal to the height of one monolayer of Pt. Furthermore, the corrugation on top of the island presents the same periodicity (d = 3 nm) and height (h = 0.36 Å) as the Ru(0001) supported graphene layer. Similar observations for Pt-gr/Ru(0001) electrodes which were annealed to temperatures above T = 800 K were reported by Huang et al., who rationalized this observation by an intercalation of Pt between the graphene layer and the Ru(0001) substrate.[21] Therefore, we conclude that also the 1 ML high islands for our electrode **6** are intercalated between the graphene layer and Ru(0001). Since these graphene-covered 1ML high Pt islands are presumed to be inactive for adsorption (as it is the case for graphene-covered Ru(0001), Fig. S2), they were excluded for

the statistical analysis of the NC height distribution in the main text and the determination of the ECSA. The trend in the normalized electrode activity for the HER (see Fig. 2 in the main text) support the correctness of this assumption.

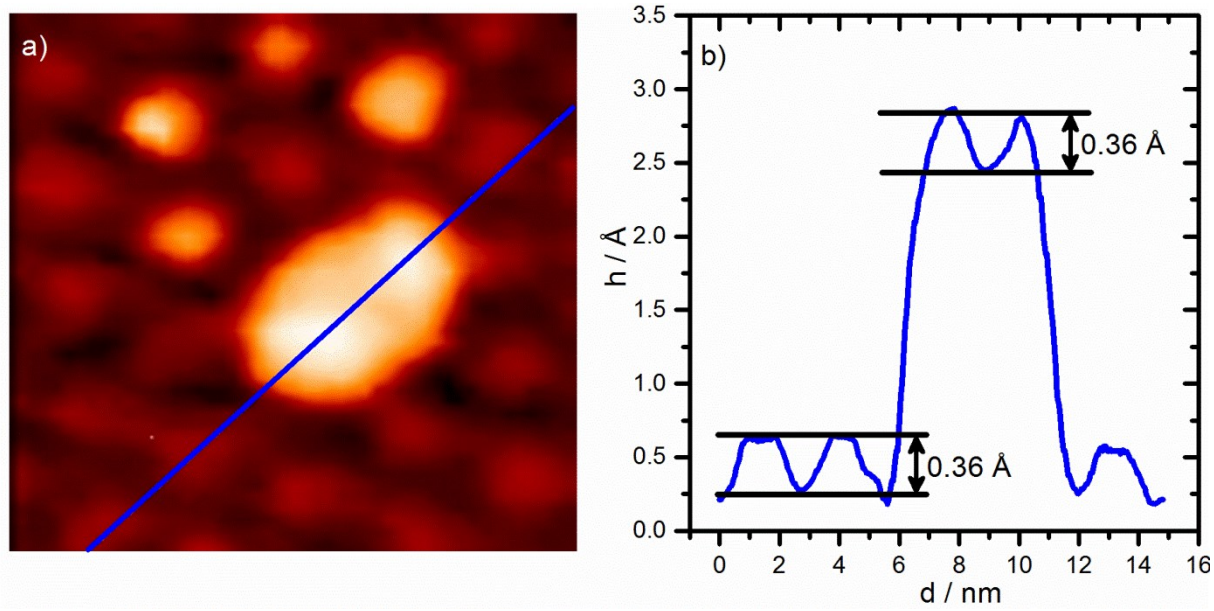

Figure S4: (**a**) Zoom in of a STM image from a monolayer high Pt-island of electrode **6** which was annealed to 873 K (15 nm x 15 nm). (**b**) Height profile along the blue line in a). The black horizontal bars indicate the presence of the same corrugation on top of the Pt-island as it appears for the Ru(0001) supported graphene sheet.

5 Electrochemical Surface Area (ECSA)

The electrochemical surface area (ECSA) is defined as the active area of the electrode surface which is exposed to the electrolyte and contributes to the electrocatalytic reaction. The methodology employed to determine the ECSA for the gr/Ru(0001) support and bulk polycrystalline Pt electrodes, serving as reference sample, is described in section 5.1. The evaluation of the ECSA for the Pt NCs, which includes the development of cluster models, is described in section 5.2.

5.1 ECSA of gr/Ru(0001) and polycrystalline Pt

The preparation of gr/Ru(0001) under UHV conditions provides a surface with terraces of widths up to 500 nm and, besides the small graphene corrugation, the surface can be assumed to be flat. In this case, the geometrical area A_{geom} can be employed as ECSA. A_{geom} is determined by the inner diameter of the O-ring of the electrochemical flow cell onto which the electrode prepared under UHV conditions is pressed. The diameter of the pressed O-ring is d = 6.0 mm and therefore $ECSA_{gr/Ru(0001)}$ = 0.28 cm². Bulk polycrystalline Pt (Pt-poly) served as a reference electrode for the properties of bulk Pt towards the HER. Its ECSA was determined with the method described by Biegler et al., [22] by a coulometric analysis of the underpotential hydrogen (H_{upd}) region from cyclic voltammograms in supporting electrolyte. As a result an $ECSA_{Pt\text{-}poly}$ = 0.874 ± 0.027 cm² was determined.

5.2 ECSA of Pt NCs

For the Pt NCs the latter method to determine $ECSA_{Pt}$ *via* the H_{upd} region is not applicable, since the H_{upd} region is not present due to the early onset of the HER. Therefore, the $ECSA_{Pt}$ of the Pt-gr/Ru(0001) electrodes were determined by the design of cluster models of the Pt NCs for which the atom composition and surface dispersion are well-known. For the design

of the cluster models the following procedure was performed separately for each of the six Pt-gr/Ru(0001) electrodes.

At first, the amount of Pt (ϑ_{Pt}) which was deposited on gr/Ru(0001) was used to determine the total number of Pt atoms ($N_{Pt,theo}$) within a 30 nm x 30 nm Moiré unit cell:

$$N_{Pt,theo} = \Theta_{Pt} \cdot A_{30x30} \cdot \varrho_{Pt}$$

where A_{30x30}= 779.4 nm² is the surface area of the Moiré unit cell and ρ_{Pt}= $1.51 \cdot 10^{15}$ atoms cm^{-2} is the atom density of the close-packed (111) surface on the Ru(0001) substrate. The term ($A_{30x30} \cdot \rho_{Pt}$) is equivalent to a full monolayer coverage inside the Moiré unit cell. Since θ_{Pt} represents the fraction of the area covered with Pt, $N_{Pt,theo}$ equals the number of Pt atoms which are actually available to form clusters inside the Moiré unit cell. The 30 nm x 30 nm unit cell contains exactly one hundred adsorption sites.[23]

The cluster models are designed in a way that the total number of atoms used to design the NCs ($N_{Pt,model}$) within a Moiré unit cell is equal to $N_{Pt,theo}$. $N_{Pt,model}$ itself is given by:

$$N_{Pt,model} = \sum_{i\,ML_{Pt}} N_{i\,ML_{Pt}} \cdot N_{i\,ML_{Pt},30x30}$$

where $N_{i\,ML_{Pt}}$ is the number of volume atoms to form a NC of i ML_{Pt} height. $N_{i\,ML_{Pt},30x30}$ is the respective number of NCs of i ML_{Pt} height within a Moiré unit cell. The value of the latter is obtained by

$$N_{i\,ML_{Pt},30x30} = n_{i\,ML_{Pt}} \cdot FF$$

where $n_{i\,ML_{Pt}}$ is the fraction of a NC with a height of i ML_{Pt} from the total amount of NCs on the Pt-gr/Ru(0001) sample. $n_{i\,ML_{Pt}}$ is obtained from the respective height distribution of each sample. Since within a Moiré unit cell there are exactly one hundred adsorption sites, the multiplication with the respective FF directly provides $N_{i\,ML_{Pt},30x30}$.

The cluster models were then designed such that $N_{Pt,model} \approx N_{Pt,theo}$ is true for all six Pt-gr/Ru(0001) electrodes. Two main criteria for the design have been that i) the NCs consist of as many fcc-sites as possible, since this is the thermodynamically most favorable facet for Pt, and ii) the surface dispersion d_{OF} decreases with increasing NC size.

Based on these cluster models the total number of Pt surface atoms ($N_{Pt\text{-}surf}$) at a Pt-gr/Ru(0001) electrode was then derived by

$$N_{Pt-surf} = \sum_{i\,ML_{Pt}} N_{OF,i\,ML_{Pt}} \cdot N_{i\,ML_{Pt},30x30}$$

where $N_{OF,i\,ML_{Pt}}$ is the number of surface atoms of a cluster model with i ML_{Pt} height. The *ECSA* of a Pt-gr/Ru(0001) sample is finally given by

$$ECSA_{Pt-Cluster} = \frac{N_{Pt-surf}}{A_{30x30} \cdot \rho_{Pt}} \cdot A_{geom}$$

The ratio between $N_{Pt\text{-}surf}$ and ($A_{30x30} \cdot \rho_{Pt}$) gives the percentage of Pt surface atoms on the substrate. The product of this percentage with A_{geom} which is the geometrical area of the sample finally leads to $ECSA_{Pt\text{-}Cluster}$.

The ECSAs for all six Pt-gr/Ru(0001) electrodes are listed in the main text in Table 1.

6 Pt NC stability

The first three HER polarization cycles of each of the six different Pt-gr/Ru(0001) electrodes are depicted in Figure S5. Regardless of the average Pt NC size the activity for the HER decreases with consecutive cycling. The extent of this deactivation varies, however, with NC size. While all electrodes except the one with Pt_{49} NCs reveal only a slight deactivation the electrode with Pt_{49} NCs exhibits a strong deactivation in the second cycle which we tentatively explain by the formation of a H_2 bubble in the EC flow cell during the first cycle leading to a reduced electrode surface area. The slight decrease of all other electrodes might be explained by dissolution or ripening of the Pt NCs resulting in a lower Pt surface area and thus in lower HER currents. STM images recorded after the HER are shown in Figure S6a and S6b demonstrating the existence of NCs also during / after the HER. The respective height distributions are shown in Figure S6c and S6d in comparison with the height distributions before the HER. After the HER the distribution is broadened and also shifted to higher NCs. This might be explained by a ripening of the NCs during the HER, however, also molecules on top of the NCs which were adsorbed in the electrochemical environment might be a reason for this larger apparent heights.

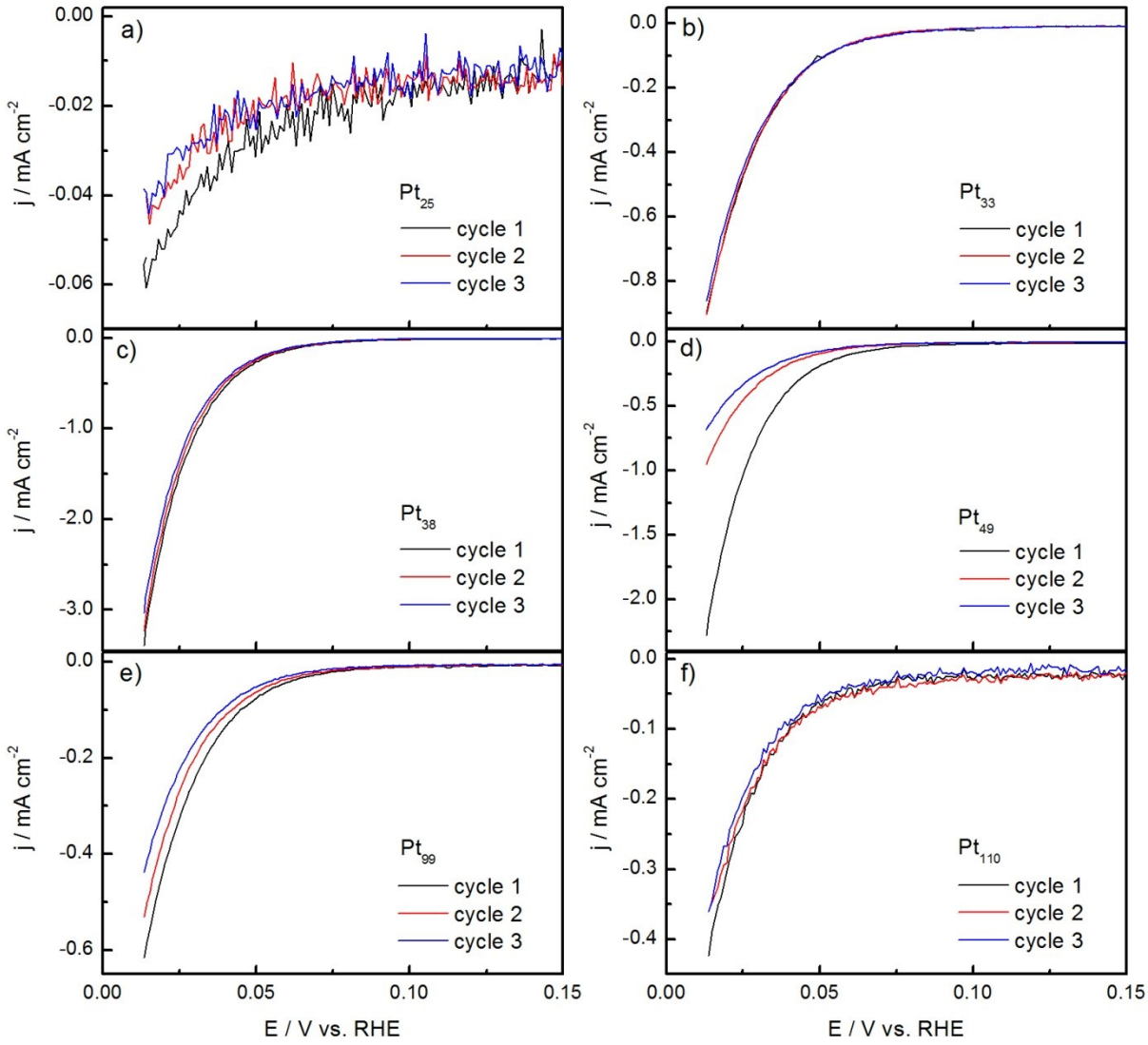

Figure S5: First three potentiodynamic HER cycles (0.01 V - 0.90 V, 0.5 M H_2SO_4, 10 mV s^{-1}), on the Pt-gr/Ru(0001) electrodes with a) Pt_{25} NCs, b) Pt_{33} NCs, c) Pt_{38} NCs, d) Pt_{49} NCs, e) Pt_{99} NCs and f) Pt_{110} NCs.

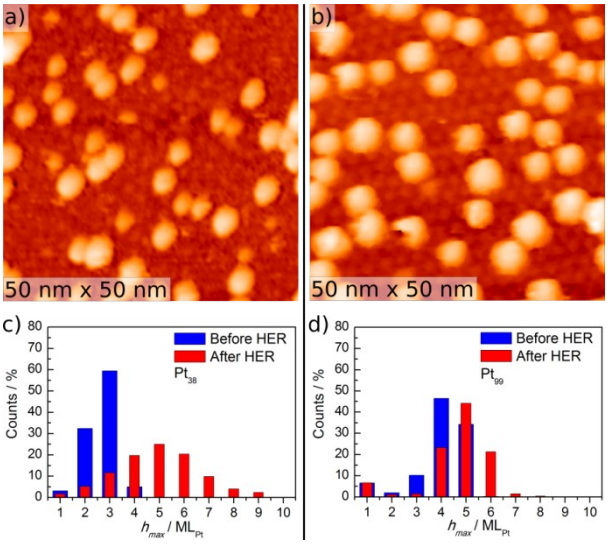

Figure S6: Representative STM images of the Pt-gr/Ru(0001) electrodes with a) Pt_{38} NCs and b) Pt_{99} NCs recorded after the HER on these electrodes. The respective height distributions before the HER (blue) and after the HER (red) are illustrated in c) (Pt_{38}) and d) (Pt_{99}).

7 Reproducibility

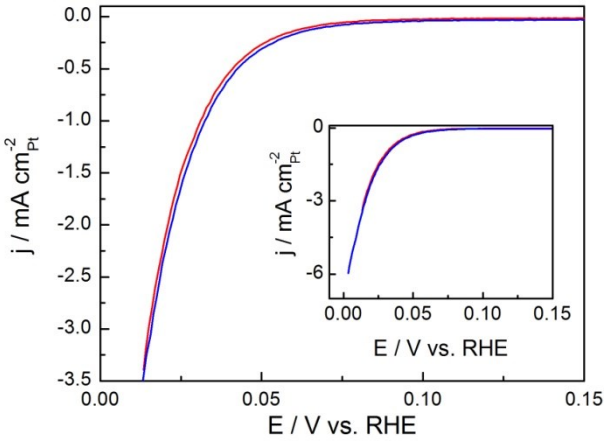

Figure S7: Potentiodynamic HER curves of two different Pt-gr/Ru(0001) electrodes with Pt_{38} NCs recorded on different measurement days (10 mV s^{-1}, 0.5 M H_2SO_4). The lower potential limits are 0.00 V and 0.01 V, respectively.

8 Tafel analysis

Tafel plots of each Pt-gr/Ru(0001) electrode and of Pt-poly are shown in Fig. S84. The Tafel slopes vary in the range between 34 mV/dec and 38 mV/dec for the different electrodes. For the most active electrode with Pt_{38} NCs the Tafel slope is 34 mV/dec (see also Table S3). The exchange current densities, which are plotted in Fig. 2b in the main text, are also given in Table S3.

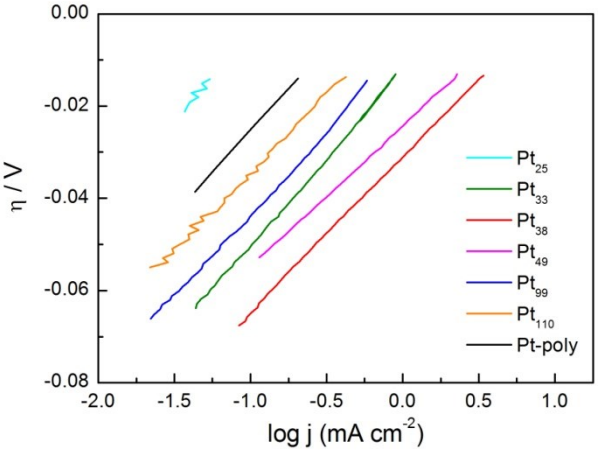

Figure S8: Tafel plots of the Pt NCs and Pt-poly: Overpotential η for the HER as a function of the logarithm of the experimentally measured current density related to the HER.

Table S3: Tafel analysis of the Pt-gr/Ru(0001) electrodes and of Pt-poly.

Electrode	S_{av} [atoms]	b [mV/dec]	j_0 [mA cm^{-2}]
1	25	37 ± 3	0.1 ± 0.1
2	33	38 ± 3	2.0 ± 0.1
3	38	34 ± 3	10.1 ± 0.1
4	49	35 ± 3	6.2 ± 0.1
5	99	36 ± 3	1.5 ± 0.1
6	110	34 ± 3	1.0 ± 0.1
Pt-poly		36 ± 3	1.0 ± 0.1

Average number of Pt atoms per cluster (S_{av}), Tafel slope (b) and exchange current density (j_0) for the different electrodes.

References

1 M. Zhou, S. Bao, A. J. Bard, *J.Am.Chem.Soc.*, 2019**, 141***,* 7327-7332.

2 F. Neuberger, J. Baranyai, T. Schmidt, T. Cottre, B. Kaiser, W. Jaegermann, R. Schäfer, *Z.Phys.Chem.*, 2019**, 2019***,* 1-19.

3 H. Tsunoyama, Y. Yamane, C. Zhang, M. Komori, T. Eguchi, A. Nakajima, *Top.Catal.*, 2018**, 61***,* 126-135.

4 Y. Takasu, Y. Fujii, K. Yasuda, Y. Iwanaga, Y. Matsuda, *Electrochim.Acta*, 1989**, 34***,* 453-458.

5 J. Durst, C. Simon, A. Siebel, P. J. Rheinländer, T. Schuler, M. Hanzlik, J. Herranz, F. Hasché, H. A. Gasteiger, *ECS Trans.*, 2014**, 64***,* 1069-1080.

6 N. Cheng, S. Stambula, D. Wang, M. N. Banis, J. Liu, A. Riese, B. Xiao, R. Li, T. K. Sham, L. M. Liu, *Nat.Commun.*, 2016**, 7***,* 13638.

7 D. J. Ham, R. Ganesan, J. S. Lee, *Int.J.Hydrogen Energy*, 2008**, 33***,* 6865-6872.

8 M. Tavakkoli, N. Holmberg, R. Kronberg, H. Jiang, J. Sainio, E. I. Kauppinen, T. Kallio, K. Laasonen, *ACS Catal.*, 2017**, 7***,* 3121-3130.

9 L. Zhang, L. Han, H. Liu, X. Liu, J. Luo, *Angew.Chem.Int.Ed.*, 2017**, 56***,* 13694-13698.

10 S. Ye, F. Luo, Q. Zhang, P. Zhang, T. Xu, Q. Wang, D. He, L. Guo, Y. Zhang, C. He, X. Ouyang, M. Gu, J. Liu, X. Sun, *Energy Environ.Sci.*, 2019**, 12***,* 1000-1007.

11 S. Anantharaj, P. E. Karthik, B. Subramanian, S. Kundu, *ACS Catal.*, 2016**, 6***,* 4660-4672.

12 A. B. Soliman, M. H. Hassan, T. N. Huan, A. A. Abugable, W. A. Elmehalmey, S. G. Karakalos, M. Tsotsalas, M. Heinle, M. Elbahri, M. Fontecave, M. H. Alkordi, *ACS Catal.*, 2017**, 7***,* 7847-7854.

13 P. Wang, X. Zhang, J. Zhang, S. Wan, S. Guo, G. Lu, J. Yao, X. Huang, *Nat.Commun.*, 2017**, 8***,* 14580.

14 J. Schnaidt, S. Beckord, A. K. Engstfeld, J. Klein, S. Brimaud, R. J. Behm, *Phys.Chem.Chem.Phys.*, 2017**, 19***,* 4166-4178.

15 A. K. Engstfeld, J. Klein, S. Brimaud, R. J. Behm, *Surf.Sci.*, 2015**, 631***,* 248-257.

16 Y. Pan, M. Gao, L. Huang, F. Liu, H.-J. Gao, *Appl.Phys.Lett.*, 2009**, 95***,* 093106.

17 A. K. Engstfeld, S. Beckord, C. D. Lorenz, R. J. Behm, *ChemPhysChem*, 2012**, 13***,* 3313-3319.

18 K. Donner, P. Jakob, *J.Chem.Phys.*, 2009**, 131***,* 164701.

19 X. Liu, Y. Han, J. W. Evans, A. K. Engstfeld, R. J. Behm, M. C. Tringides, M. Hupalo, H. Q. Lin, L. Huang, K. M. Ho, D. Appy, P. A. Thiel, C. Z. Wang, *Prog.Surf.Sci.*, 2015**, 90***,* 397-443.

20 Z. Zhou, F. Gao, D. W. Goodman, *Surf.Sci.*, 2010**, 604***,* L31-L38.

21 L. Huang, Y. Pan, L. Pan, M. Gao, W. Xu, Y. Que, H. Zhou, Y. Wang, S. Du, H. J. Gao, *Appl.Phys.Lett.*, 2011**, 99***,* 163107.

22 T. Biegler, D. A. J. Rand, R. Woods, *J.Electroanal.Chem.*, 1971**, 29***,* 269-277.

23 B. Wang, M. L. Bocquet, S. Marchini, S. Gunther, J. Wintterlin, *Phys.Chem.Chem.Phys.*, 2008**, 10***,* 3530-3534.